ACCSCIENCE PUBLISHING

International Journal of Bioprinting

RESEARCH ARTICLE

Boronate ester–crosslinked GelMA composite bioink for 3D bioprinting of cell-laden corneal stroma and *in vivo* evaluation in rabbits

Yi-Jen Hsueh[1,2†], Chung-An Chen[3,4,5†], Chin-Yu Yang[2], Chang-Hong Lin[1], Chun-Yuan Cheng[5], Chih-Hsin Lin[6,7,8], Shih-Jung Liu[5,9], Tsung-Ting Tsai[3,4,5*], and Hung-Chi Chen[1,2,3*]

[1]Department of Ophthalmology, Chang Gung Memorial Hospital, Linkou Branch, Taoyuan, Taiwan

[2]Center for Tissue Engineering, Chang Gung Memorial Hospital, Linkou Branch, Taoyuan, Taiwan

[3]Department of Medicine, College of Medicine, Chang Gung University, Taoyuan, Taiwan

[4]Department of Orthopaedic Surgery, Chang Gung Memorial Hospital, Linkou Branch, Taoyuan, Taiwan

[5]Spine Section and Bone and Joint Research Center, Chang Gung Memorial Hospital, Taoyuan, Taiwan

[6]Institute of Molecular Medicine and Bioengineering, National Yang Ming Chiao Tung University, Hsinchu, Taiwan

[7]Department of Dentistry, School of Dentistry, National Yang Ming Chiao Tung University, Taipei, Taiwan

[8]Department of Biological Science and Technology, College of Engineering Bioscience, National Yang Ming Chiao Tung University, Hsinchu, Taiwan

[9]Department of Mechanical Engineering, College of Engineering, Chang Gung University, Taoyuan, Taiwan

[†]*These authors contributed equally to this work.*

***Corresponding authors:**
Hung-Chi Chen (mr3756@cgmh.org.tw);
Tsung-Ting Tsai (tsai1129@gap.cgu.edu.tw)

Citation: Hsueh YJ, Chen CA, Yang CY, *et al*. Boronate ester–crosslinked GelMA composite bioink for 3D bioprinting of cell-laden corneal stroma and *in vivo* evaluation in rabbits. *Int J Bioprint*. 2026;12(5):026350379. doi: 10.36922/IJB026350379

Received: February 3, 2026

1st revised: August 28, 2026

2nd revised: September 12, 2026

Accepted: September 15, 2026

Published online: September 15, 2026

Copyright: © 2026 Author(s). This is an Open-Access article distributed under the terms of the Creative Commons Attribution License, permitting distribution, and reproduction in any medium, provided the original work is properly cited.

Publisher's Note: AccScience Publishing remains neutral with regard to jurisdictional claims in published maps and institutional affiliations.

Abstract

Corneal transplantation restores vision by replacing damaged corneal tissue with a donor graft, but the limited supply and variable quality of donor corneas remain major challenges. We therefore developed an engineered corneal substitute using gelatin methacryloyl (GelMA), a modified gelatin. Phenylboronic acid–functionalized gelatin (PBA@G) and poly(vinyl alcohol) (PVA) were incorporated to introduce dynamic boronate ester crosslinking and modify the rheological behavior of the hydrogel. The optimized bioprinting formulation contained 10% GelMA, 10% PBA@G, and 1% PVA (10G10P1PVA). Scanning electron microscopy revealed an interconnected porous microstructure. The rheological behavior, optical transmittance, swelling, degradation, and printability of 10G10P1PVA were characterized. Human corneal stromal cells remained viable through day 7, and the Cell Counting Kit-8 assay showed significantly higher metabolic activity in 10G10P1PVA than in 10G. Phalloidin staining showed cell spreading and longitudinal F-actin organization. Quantitative real-time polymerase chain reaction showed no marked *ACTA2* induction, with expression remaining below that of the myofibroblast-like reference group. The corneal stromal cell marker *ALDH3A1* was expressed at higher levels in cells cultured in 10G10P1PVA than in either the 10G or 10G10P group. These findings support the short-term cytocompatibility of the newly developed bioink and selected stromal-associated features. An exploratory rabbit anterior lamellar keratectomy evaluation was performed to document short-term ocular response, epithelial recovery, and stromal organization following implantation over seven days. Together, the material

and biological results support further evaluation of 10G10P1PVA as a GelMA-based composite bioink for corneal stromal bioprinting.

Keywords: Artificial corneal stroma; Bioink; Bioprinting; Biomaterials; Photocrosslinking; 3D cell culture

1. Introduction

The cornea is the transparent anterior tissue of the eye and provides the principal refractive surface through which light enters the eye. Irreversible disruption of corneal structure or transparency can result in severe visual impairment or blindness. For advanced corneal diseases in which transparency and visual function cannot be restored by other treatments, corneal transplantation remains the mainstay of treatment. However, the global supply of donor corneas falls far short of clinical demand. A global survey by Gain *et al.*[1] estimated that approximately 12.7 million patients were awaiting corneal transplantation, with only one donor cornea available for every 70 needed and approximately 53% of the world's population lacking access to corneal transplantation services. In its 2022 Package of Eye Care Interventions, the World Health Organization also highlighted limitations in corneal donation, eye-banking capacity, and access to transplantation services in many countries. The persistent shortage of donor corneas therefore remains a major clinical driver for developing tissue-engineered corneal substitutes and bioengineered artificial corneas.[2]

The development of artificial corneas has spanned more than two decades.[3] Various materials and techniques have been developed, including poly(ethylene glycol), polycaprolactone, poly(vinyl alcohol) (PVA), and poly(lactic-co-glycolic acid), as well as natural macromolecules such as collagen, gelatin, alginate, and hyaluronic acid, to create functional tissues that can replace natural corneas. Additionally, decellularized corneas and self-assembled molecules have been explored. Recently, corneal bioprinting has been used to evaluate corneal tissue repair and replacement. An early report by Kim[4] in 2014 described a 3D-bioprinted corneal stromal prototype using fibrinogen–hyaluronic acid hydrogel and limbal keratocytes. The results revealed that the cells resembled *in vivo* human stromal tissue both morphologically and biologically. A key consideration in corneal bioprinting is the bioink, which must balance optical transmittance, physicochemical properties, and biomechanical performance. Gelatin methacryloyl (GelMA) is a modified form of gelatin that offers excellent biocompatibility, easy customization, and broad applicability. GelMA-based hydrogels are biocompatible, biodegradable, noncytotoxic, and nonimmunogenic, making them well suited for biomedical applications. The 3D network structure of GelMA mimics that of the natural extracellular matrix, creating an ideal environment for 3D cell growth. Additionally, GelMA is a versatile biomaterial that can be modified as needed for specific applications.[5] The compressive modulus of GelMA can be precisely tuned by adjusting the level of methacryloyl substitution or by adding inorganic or organic additives.[6] Corneal stromal biofabrication has progressed from early collagen-based cell-laden constructs[7,8] to GelMA-based and composite hydrogel systems, including conventional GelMA,[9] fiber-reinforced GelMA,[10] corneal decellularized extracellular matrix–GelMA,[11] GelMA/collagen,[12] and GelMA/carboxymethyl chitosan formulations.[13] These studies have demonstrated advances in printability, optical properties, stromal cell phenotype, stromal architecture, and *in vivo* tissue response, with preclinical evaluation of 3D-printed cell-laden corneal constructs in rabbit models also reported.[14,15] Collectively, these findings highlight the need to balance printability, optical transparency, material properties, and stromal cell responses when designing bioinks for corneal stromal engineering.

To improve the mechanical strength of biomaterials, several strategies can be employed, such as polymer crosslinking,[16,17] using composite material structures,[18,19] and introducing dynamic chemical bonds.[20-22] Among these methods, biomaterials with dynamic covalent bonds have attracted significant attention because of their self-healing ability and potential for fabrication and synthesis. These materials can exhibit various advanced properties, including self-healing and shape memory, increased toughness, stress relaxation, and the ability to transition between different macromolecular architectures.[23] Numerous examples of dynamic covalent bonds suitable for self-healing polymers include oxime, acylhydrazone, imine, disulfide, and boronic/boronate ester bonds.[24] Boronic/boronate esters are formed through reactions between boronic acid and 1,2- or 1,3-diols, generating boron–oxygen (B–O) bonds. Recently, some natural polymers and hydrogels have been modified with boronic/boronate esters to improve mechanical strength, making them more resilient and durable and broadening their applications in structural materials.

The success of corneal bioprinting depends not only on the physicochemical properties of the scaffold but also on the phenotype of the incorporated corneal stromal cells (CSCs). During *in vitro* culture, CSCs may undergo phenotypic activation toward fibroblastic or myofibroblastic states, particularly under serum-rich conditions.[25] Myofibroblastic activation is characterized by increased expression of alpha-smooth muscle actin (α-SMA), whereas less activated stromal cells retain greater expression of keratocyte-associated proteins, including corneal crystallins such as aldehyde dehydrogenase 3 family member A1 (ALDH3A1). Phenotypic activation is also accompanied by changes in extracellular matrix remodeling and matrix metalloproteinase (MMP) activity.[26] Although maintaining a keratocyte-associated phenotype during *in vitro* expansion remains challenging, culture conditions that limit myofibroblastic activation may help preserve a less activated stromal phenotype. Binte *et al.*[25] reported that modulation of serum concentration and supplementation with amniotic membrane–derived factors can help preserve keratocyte-associated characteristics during CSC culture. In the present study, CSC phenotype was therefore evaluated, in addition to cell viability, as a complementary biological parameter relevant to the development of cell-laden corneal constructs.

This study aims to develop and characterize a composite hydrogel based on boronic/boronate ester chemistry for corneal bioprinting and 3D cell culture. GelMA, phenylboronic acid–functionalized gelatin (PBA@G), and PVA were combined to generate a photocrosslinkable formulation, and its rheological behavior, transparency, handling characteristics, and cytocompatibility were evaluated. The resulting 10G10P1PVA formulation was the primary focus of this study. To further assess its applicability as a cell-laden construct, CSC viability, cytoskeletal organization, and phenotype-associated marker expression were evaluated. Finally, a rabbit anterior lamellar keratectomy (ALK) model was used for a preliminary *in vivo* evaluation of early ocular response and the potential contribution of incorporated CSCs to corneal repair.

2. Materials and methods

2.1. Materials

Gelatin from porcine skin, PVA, phenylboronic acid (PBA), N-hydroxysuccinimide (NHS), N-(3-dimethylaminopropyl)-N'-ethylcarbodiimide hydrochloride (EDC), dimethyl sulfoxide (DMSO), sodium bicarbonate, sodium chloride (NaCl), methacrylic anhydride (MAA), glycine, deuterium oxide (D_2O), and 2,4,6-trinitrobenzenesulfonic acid (TNBS) solution (5% w/v in water) were purchased from Sigma-Aldrich (United States of America [USA]). Hydrochloric acid (HCl), sodium dodecyl sulfate (SDS), and sodium hydroxide (NaOH) were purchased from J.T. Baker (USA). N-morpholinoethanesulfonic acid (MES) was purchased from Acros Organics (Belgium). 2-Hydroxy-4′-(2-hydroxyethoxy)-2-methylpropiophenone (Irgacure 2959) was purchased from Tokyo Chemical Industry Co., Ltd. (Japan). Collagenase IV was purchased from Worthington Biochemical Corp. (USA). Dialysis bags (molecular weight cutoffs of 3.5 and 12–14 kDa) were purchased from Rainbow Biotechnology (Taiwan). A Millex-HA Filter Unit for a 33-mm-diameter sterile syringe filter with a 0.45-μm pore size mixed cellulose ester membrane was purchased from Merck (Germany). Dulbecco's phosphate-buffered saline, Dulbecco's modified Eagle's medium: nutrient mixture F-12 (DMEM/F12), fetal bovine serum (FBS), phosphate-buffered saline (PBS), and penicillin–streptomycin were purchased from Gibco (USA). Double-distilled water was obtained using an Arium Advance Pure Water System (Sartorius, Germany) and prepared with a minimum resistivity of 18.2 MΩ·cm.

2.2. Synthesis of GelMA and PBA@G

Gelatin was modified with MAA using an alkaline buffer solution, as described by Chou *et al.*[27,28] and Shirahama *et al.*[27,28], with slight modifications. In brief, gelatin (type A, 300 bloom) was dissolved in carbonate–bicarbonate (CB) buffer (250 mM, pH 9) and stirred at 50 °C until the solution was uniform. Next, MAA (10% w/v; 0.04 mL per gram of gelatin) was added to the gelatin solution, which was magnetically stirred at 500 rpm for 3 h. The pH was then adjusted to 7.4 with 6 N HCl to halt the reaction. After filtration, dialysis with Slide-A-Lyzer cassettes, and lyophilization, the GelMA samples were stored at −20 °C until further use.

PBA@G was synthesized by modifying gelatin with PBA through an NHS/EDC-mediated carbodiimide crosslinking reaction, following the procedure of Liu *et al.*[29] with slight modifications. First, 1.0 g of gelatin was dissolved in 50 mL of pure water in a 45 °C bath. Additionally, 100.0 mg of PBA, 50 mg of NHS, and 100 mg of EDC were dissolved in 3 mL of DMSO at 60 °C for 5 h for activation. The activated PBA solution was then added dropwise to the gelatin solution, and the reaction proceeded for 24 h in a 37 °C oven. The product was dialyzed in a dialysis bag (molecular weight cutoff of 3.5 kDa) for 4–5 days to remove side products, then freeze-dried and lyophilized (HyperCOOL HC3055; LabTech Srl, Italy) for 3 days to yield a foam-like powder, which was stored at −20 °C.

2.3. Fabrication of a photocrosslinking device and mixing the hydrogel with a photoinitiator

A custom 3D-printed UV light–emitting device was fabricated to provide 365-nm illumination for photocrosslinking (Figure S1). The housing was printed from polylactic acid using an Ender-3 V2 printer (Creality 3D, China), and a modular light-emitting diode (LED) was mounted and secured in the device.

For photocrosslinking, GelMA (20% w/v), PBA@G (20% w/v), and PVA (2% w/v) were dissolved in ultrapure water to prepare a polymer precursor solution. An Irgacure 2959 solution (2% w/v) was then mixed with the precursor at a 1:1 (v/v) ratio. The resulting working solution was vortexed for 30 s and incubated at 40 °C for at least 20 min. The precursor containing 1% Irgacure 2959 underwent sol–gel transition within 2 min under 365-nm irradiation.

2.4. Nuclear magnetic resonance spectroscopy, Fourier transform infrared spectroscopy, and scanning electron microscopy

To verify substitution, 1H nuclear magnetic resonance (NMR) spectroscopy was performed as previously described.[27] The gelatin, GelMA, and PBA@G samples were each dissolved to a concentration of approximately 20 mg/mL in deuterium oxide. The chemical shifts of each sample were measured at 37 °C using a 600 MHz NMR spectrometer (AVANCE III HD 600, Switzerland).

The compositions of the gelatin, GelMA, and PBA@G samples were examined with an Agilent Cary 630 Fourier transform infrared (FTIR) instrument (Agilent Technologies Inc., USA) between 4,000 and 650 cm^{-1} in attenuated total reflection mode at room temperature.

Scanning electron microscopy (SEM) was used to compare the microstructures of the crosslinked 10G, 10G10P, and 10G10P1PVA hydrogels. The hydrogels were photocrosslinked after mixing with 1% Irgacure 2959 and exposure to 365 nm UV light for 2 min. The samples were then frozen for 2 days at −80 °C, followed by lyophilization at −50 °C for 3 days to obtain foamy fragments. SEM images were obtained via field-emission SEM (FE-SEM) (Hitachi SU8220, Japan).

2.5. Determination of the degree of functionalization

To quantify the degree of functionalization (DoF), a TNBS assay was performed following the method of Habeeb,[28,30] as modified by Shirahama *et al.*[28] In brief, the GelMA and gelatin samples were separately dissolved in 0.1 M sodium bicarbonate buffer (pH 8.5) to a concentration of 1.6 mg/mL. Each solution (250 µL) was then mixed with a 0.2% TNBS solution (in 0.1 M sodium bicarbonate buffer), and the mixture was incubated at 37 °C for 3 h. Next, 250 µL of 10% w/v SDS and 125 µL of 1 M HCl were added to each solution to stop the reaction. The absorbance of each sample was measured at 335 nm. A standard curve of glycine was then plotted to determine the amino group concentration in the sample solutions at concentrations of 0, 0.8, 8, 16, 32, and 64 µg/mL.

2.6. Rheological analysis

The rheological properties of the gelatin, GelMA, and PBA@G hydrogels were assessed using an MCR 302e rheometer (Anton Paar Physica, Germany) with a PP25 Measuring Parallel Plate accessory at DG26.7. The cylinder was tested with the P-PTD220 Air and C-PTD 200 Heating rheometer systems. The experimental conditions included a shear rate of 0.1 to 100 s^{-1} at 20 °C for the flow curve, an amplitude sweep with 0.01% to 1,000% shear strain at an angular frequency of 10 s^{-1} at 20 °C, and a shear strain of 2% at a frequency of 1 Hz over the temperature range of 20 °C to 40 °C.

2.7. Transparency, degradation, and swelling tests

Optical transmittance of photocrosslinked 10G10P1PVA containing 1% Irgacure 2959 was measured at 37 °C using a Synergy HTX Multi-Mode Reader (Agilent Technologies, Inc.). A 120 µL aliquot of the hydrogel sample was added to each well of a 96-well microplate (Corning 3635, Corning Inc., USA), resulting in a hydrogel thickness of approximately 3.8 mm. Absorbance was spectrally scanned from 400 to 700 nm. A photograph showing the visibility of letters through the hydrogel was retained as a qualitative reference. The transmittance was determined using **Equation 1**:

$$\text{Transmittance (\%)} = 10^{(2-A)} \quad (1)$$

For the *in vitro* degradation assay, approximately 300 µL of each hydrogel sample was lyophilized and weighed as *M0*. The samples were then incubated at 37 °C in 1× PBS (pH 7.4) containing 20 µg/mL type IV collagenase. At each time point, the samples were removed, washed with pure water, lyophilized, and weighed as *Mt*. The degradation rate was determined using **Equation 2**:

$$\text{Degradation rate (\%)} = \frac{M0 - Mt}{M0} \times 100\% \quad (2)$$

The swelling properties of the hydrogels were evaluated using lyophilized samples of 10% GelMA, 10G10P, and 10G10P1PVA. The initial dry weight of each sample was recorded as W_d. The samples were immersed in double-distilled water at room temperature for 24 h, then removed

from the solution. Excess surface liquid was gently removed, and the swollen samples were immediately weighed to obtain the swollen weight (W_s). The swelling ratio was calculated using **Equation 3**:

$$\text{Swelling ratio (\%)} = \frac{W_s - W_d}{W_d} \times 100\% \quad (3)$$

2.8. Human corneal stromal cell preparation

Human corneal keratocytes were purchased from Innoprot (P10972; Spain) and used as human CSCs. Cells were initially maintained in DMEM/F12 supplemented with 2% FBS, 1% insulin–transferrin–selenium (ITS; Sigma-Aldrich), 1.25 μg/mL amphotericin B (Invitrogen), 25 μg/mL gentamicin (Sigma-Aldrich), and 0.02 μg/mL epidermal growth factor (PeproTech, Thermo Fisher Scientific, USA). Upon reaching approximately 50% confluence, the cells were cultured under two different conditions to generate distinct phenotypic states. CSCs maintained under conditions designed to limit myofibroblastic activation were designated CSC-F, whereas CSCs cultured under conditions intended to induce a myofibroblast-like phenotype were designated CSC-M. The CSC-F culture condition was adapted from the approach described by Binte *et al.*[25] For CSC-F preparation, cells were cultured in DMEM/F12 supplemented with 5% FBS, 10 μM SB431542 (Sigma-Aldrich), 10 μM Y27632 (Sigma-Aldrich), and 5 μg/mL amniotic stromal extract. For CSC-M induction, cells were cultured in DMEM/F12 supplemented with 10% FBS. The phenotypic differences between CSC-F and CSC-M were subsequently evaluated by cell morphology, α-SMA expression, MMP-2 secretion, and phenotype-related gene expression. Culture media and cells were collected for the corresponding downstream analyses.

2.9. Matrix metalloproteinase-2 enzyme-linked immunosorbent assay

An MMP-2 ELISA Kit (QZBmmp2Hv2, QuickZyme Bioscience, Netherlands) was used to quantify MMP-2 levels in the culture media of CSC-F and CSC-M. The standards were diluted in series, and the test samples were diluted 10-fold with assay buffer. One hundred microliters of each sample were added to the MMP-2 enzyme-linked immunosorbent assay (ELISA) plate and incubated at 4 °C overnight. The plate was subsequently washed four times with wash buffer, after which 50 μL of 4-aminophenylmercuric acetate (APMA) and 50 μL of detection solution were added to measure the T0 (0-hour) value at an optical density of 405 nm. The plate was then incubated at 37 °C for 4 h to obtain the T4 data.

2.10. Evaluation of cell viability and morphology

The artificial cornea test materials were divided into three groups: 10% GelMA (10G), 10% GelMA with 10% PBA@G (10G10P), and 10% GelMA with 10% PBA@G and 1% PVA (10G10P1PVA). CSCs at a density of 1×10^6 cells/mL were mixed with the hydrogel formulations. Cell viability was evaluated on days 0, 1, and 7 using a Live/Dead Kit (295, IMT Formosa New Materials, Taiwan), and the stained cells were examined using a confocal microscope (Leica TCS SP8X, Germany).

Cell metabolic activity was additionally assessed on day 7 using a Cell Counting Kit-8 (CCK-8) assay (291, IMT Formosa New Materials) according to the manufacturer's instructions. Absorbance was measured at 450 nm using a microplate reader, and the values were normalized to those of the 10G group.

For evaluation of cell morphology and cytoskeletal organization, cell-laden hydrogels cultured for seven days were washed with 1× PBS and fixed with 4% paraformaldehyde (PFA) containing 0.1% Triton X-100 for 60 min. After washing with PBS, the samples were permeabilized with 1% Triton X-100 in PBS for 60 min. F-actin and nuclei were subsequently stained with 1× Alexa Fluor 488 phalloidin (A12379, Thermo Fisher Scientific) and 4′,6-diamidino-2-phenylindole (DAPI) in PBS for 60 min. After washing with PBS, fluorescence images were acquired using a confocal microscope (TCS SP8X, Leica Microsystems, Germany).

2.11. Quantitative real-time polymerase chain reaction

Total RNA was isolated from the indicated CSC cultures using TRIzol reagent. Complementary DNA (cDNA) was synthesized using the PrimeScript RT Reagent Kit (RR037A, TaKaRa, Japan) according to the manufacturer's instructions. Quantitative real-time polymerase chain reaction (RT-PCR) was performed using KAPA SYBR FAST ABI Prism 2X qPCR Master Mix (KM4102, Kapa Biosystems/Roche, USA). The expression of *ACTA2* (encoding α-SMA) and *ALDH3A1* was evaluated as markers of myofibroblastic activation and corneal stromal phenotype, respectively. *ACTB* was used as the internal reference gene. Relative gene expression was calculated using the $2^{-\Delta\Delta CT}$ method. Primer sequences are listed in Table S3.

2.12. Western blotting

Cells were lysed in radioimmunoprecipitation assay (RIPA) buffer supplemented with inhibitors (10 mM NaF, 10 mM Na_3VO_4, and a 1× protease inhibitor cocktail; Sigma-Aldrich). The lysates were kept on ice, transferred to microtubes, briefly sonicated, and centrifuged at 20,800× *g* for 15 min at 4 °C. The supernatants were collected as

total protein extracts. The samples were separated by 10% acrylamide SDS–polyacrylamide gel electrophoresis (PAGE) and electrotransferred onto polyvinylidene fluoride (PVDF) membranes (MilliporeSigma, USA). The membranes were blocked with 5% skim milk in Tris-buffered saline with Tween 20 (TBST; 50 mM Tris-HCl, pH 7.5; 150 mM NaCl; 0.05% Tween-20), incubated overnight at 4 °C with the indicated primary antibodies, and then treated with the appropriate horseradish peroxidase (HRP)-linked secondary antibodies. Immunoreactive bands were visualized using enhanced chemiluminescence (ECL) reagents (GE Healthcare, United Kingdom).

The primary antibodies used were anti-α-SMA (19245S, Cell Signaling Technology, USA) and anti-GAPDH (sc-47724, Santa Cruz Biotechnology, USA). The HRP-conjugated secondary antibodies used were donkey anti-rabbit IgG (NA934V, Cytiva, United Kingdom) and sheep anti-mouse IgG (NA931V, Cytiva).

2.13. Printing the artificial cornea with a BIO X 3D printer

The artificial cornea was produced using a BIO X 3D bioprinter (Cellink, Sweden). A cornea-shaped groove mold was fabricated as the base for bioprinting (Figure S2). The scanned corneal mold was digitized and processed using 3D modeling software to generate a reverse model of the artificial cornea. Printing used a 3-mL syringe and 25 G blunt needle (nozzle diameter, 0.41 mm) at a syringe temperature of 33.5 °C, bed temperature of 15 °C, extrusion pressure of 20 psi (137.9 kPa), and printing speed of 3 mm/s; the programmed layer height was set to 50% of the nozzle diameter (0.205 mm). The construct in Figure S2F was printed as a single layer and photocrosslinked at 365 nm for 120 s. The UV wavelength and exposure time were recorded, whereas irradiation intensity was not independently measured in the present experiment.

Printing began at the center of the groove mold, within the path that expanded outward in concentric circles. After each full circle, the BIO X printer was programmed to apply UV light for 10 s to cure the printed layer before moving on to the next printing step. Finally, a transparent, concave, disc-shaped artificial cornea was printed after several cycles and stored in 1× PBS.

2.14. Animal experiments

To evaluate the effect of the cell-seeded hydrogel on corneal repair, a rabbit ALK model was established. Animal experiments were conducted in compliance with the Chang Gung Memorial Hospital Animal Research Guidelines and the Guide for the Care and Use of Laboratory Animals published by the National Institutes of Health. Ethical approval was obtained from the Institutional Animal Care and Use Committee of Chang Gung Memorial Hospital (No. 2022022303).

For the *in vivo* implantation experiments, rabbit corneal stromal cells (RCSCs) were used instead of the human CSCs employed in the *in vitro* studies to avoid xenogeneic immune responses. RCSCs were isolated from rabbit corneal tissues according to a previously described method.[31] Briefly, central corneal buttons were prepared from Descemet membrane–stripped corneas and incubated with 5 mg/mL dispase II at 4 °C overnight. After removal of the loosened epithelial sheets, the stromal discs were cut into small pieces and digested with 2 mg/mL collagenase I for 24 h at 37 °C. Cell pellets were collected by centrifugation at 1,000 rpm for 5 min at 25 °C and resuspended in RCSC medium consisting of DMEM supplemented with 10% FBS and 25 μg/mL gentamicin. The cells were cultured on FNC-coated plates at 37 °C in 5% CO_2 and subcultured for preparation of the Cell-Full constructs.

A total of eight New Zealand White rabbits were used in the animal experiments associated with this study. Three rabbits were used in preliminary implantation and procedure-development experiments and were not included in the final ALK outcome evaluation. The final exploratory ALK evaluation included five rabbits: ALK without grafting (Control, n = 1), ALK followed by transplantation of an allogeneic corneal graft (Graft, n = 2), ALK followed by implantation of a cell-free 10G10P1PVA hydrogel (Cell-Free, n = 1), and ALK followed by implantation of a 10G10P1PVA hydrogel seeded with RCSCs (Cell-Full, n = 1). Rabbits included in the final ALK evaluation weighed 3.36–4.02 kg and were anesthetized through intramuscular injection of a 1:1 mixture of Zoletil (25 mg/mL) and Rompun (10 mg/mL). The anterior corneal lamella, including the epithelium and approximately 150 μm of the anterior stroma, was excised using a 7.5-mm corneal trephine. The rabbits were divided into four ALK groups: ALK without grafting (Control) and ALK followed by transplantation of an allogeneic corneal graft (Graft), a cell-free 10G10P1PVA hydrogel (Cell-Free), or a 10G10P1PVA hydrogel seeded with RCSCs (Cell-Full). External eye photographs and fluorescein staining images were obtained immediately after ALK and treatment on day 0 to document the initial surgical defect. In all four ALK groups, the surgical site was subsequently covered with amniotic membrane and secured with 10-0 sutures for protection. The eyelids were temporarily closed with 6-0 Mersilk sutures. On day 3, the eyelid sutures and amniotic membrane were removed. Corneal recovery was subsequently evaluated through external eye photography

and fluorescein staining on days 4 and 7. Normal rabbit corneas without ALK were included as histological references.

2.15. Histological analysis

The corneas were harvested on day 7 after ALK for histological evaluation. Each sample was fixed in 10% buffered formalin for 24 h, followed by dehydration, paraffin embedding, and sectioning. The tissue sections were subjected to hematoxylin and eosin (H&E) and Masson's trichrome staining. Histological sections were examined to assess epithelial continuity, anterior corneal contour, and stromal organization among the experimental groups. Normal rabbit corneas were processed as histological references.

2.16. Statistical analysis

Quantitative data are presented as the mean ± standard deviation (SD). Statistical analyses were performed using Microsoft Excel (IBM, USA). Differences between groups were evaluated using two-tailed Student's *t*-tests. A p-value < 0.05 was considered statistically significant.

3. Results and discussion

An overview of the synthesis of GelMA and PBA@G and the *in vivo* corneal evaluation is shown in Figure 1. One-pot MAA modification of the gelatin enabled efficient, straightforward GelMA synthesis using a CB buffer system. In addition, the gelatin was modified with PBA using the EDC/NHS method to generate the final product, PBA@G, for this study. To ensure the stability and quality of the synthesized materials, we characterized the compounds using NMR, FT-IR, and SEM to confirm their formation. The rheological, transparency, swelling, and *in vitro* degradation tests provided baseline characterization of the hydrogel formulations.

3.1. Instrumentation and microscopic imaging for compound identification

^{1}H NMR spectroscopy of gelatin, GelMA, and PBA@G was performed to characterize the methacrylation, and the DoF of GelMA was quantified (Figure 2A–B). Within the GelMA sample, the three central regions were analyzed to verify successful modification: (i) the characteristic peaks at approximately 5.4 and 5.7 ppm, corresponding to the methacrylamide double bond-adjacent protons; (ii) the peak at 2.9–3.0 ppm, attributed to unreacted methylene protons from lysine residues; and (iii) the peak at 1.8–1.9 ppm, corresponding to the methacrylamide single bond-adjacent protons. Agreement between the spectra confirmed successful synthesis of GelMA.[28] In contrast, PBA@G showed distinct peaks at approximately 7.5 and 7.8 ppm, corresponding to the aromatic protons of the benzene ring. These peaks are characteristic of the aromatic hydrogens in PBA@G and are absent in the gelatin and GelMA samples, distinguishing the molecular structure of PBA@G. In the current study, the DoF was calculated for the GelMA samples.[32,33] The NMR results (DoF = 54.60%) and the TNBS assay results revealed a medium DoF of 50%–55% for GelMA (Table S1), indicating high stability and repeatability of its synthesis. According to Xie *et al.*,[34] PBA groups in different PBA@G samples cannot be well quantified through NMR; thus, determining the DoF of PBA@G was difficult. In general, GelMA can be classified into three types (low, medium, and high) depending on the DoF, with up to 40% substituted amine groups indicating a low DoF, and at least 65% substituted amine groups indicating a high DoF. The DoF significantly affects the physical properties of GelMA, including swelling, stiffness, and enzymatic degradation, with increasing functionalization generally associated with greater stiffness and slower degradation.[35-37] In this study, we referred to the methods of Liu *et al.*[29] to modify the hydrogel formulation for application in artificial corneal stroma.

Meanwhile, FTIR was also employed for chemical group identification. As shown in Figure 2C, the broad absorption band observed in the range of 3,200–3,500 cm^{-1} corresponds to the stretching vibrations of N–H and O–H bonds. Since gelatin contains amine ($–NH_2$) and hydroxyl (–OH) functional groups, a broad peak appeared in this wavenumber range for the gelatin sample.[27] All three materials (gelatin, GelMA, and PBA@G) exhibited absorption peaks within this range, indicating the presence of amine and hydroxyl groups in their structures. The spectral profiles of GelMA and gelatin are relatively similar. In contrast, the shape of the peak in the PBA@G spectrum differed from those of the other two materials, which may be attributed to changes in hydrogen-bond distribution resulting from chemical modification. The characteristic peak at 1,650 cm^{-1} (amide I band) corresponds to the C = O stretching vibration, originating from the amide bonds in gelatin. The peak located at approximately 1,650 cm^{-1} is one of the characteristic absorption bands of gelatin. The presence of this absorption peak in the gelatin, GelMA, and PBA@G samples indicates that the amide bond is retained in all three materials. The absorption peak at approximately 1,550 cm^{-1} (amide II band) is typically due to the N–H bending vibration and C–N stretching vibration, and it is characteristic of the amide bond in the gelatin structure. A slight shift in this peak was observed in the GelMA and PBA@G spectra relative to gelatin, which may reflect changes associated with their respective chemical modifications.

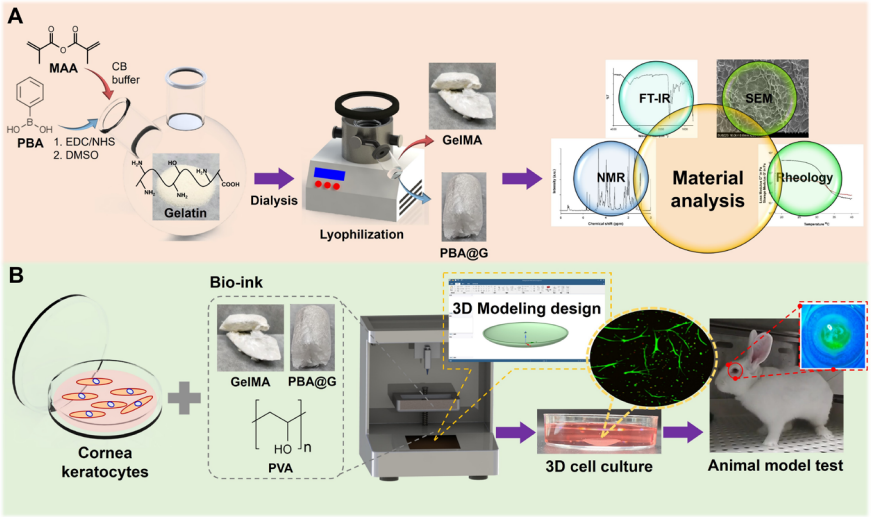


Figure 1. Overview of (A) the synthesis of GelMA and the PBA@G hydrogel and (B) the examination of their biocompatibility in a rabbit model
Abbreviations: DMSO: Dimethyl sulfoxide; EDC: N-(3-dimethylaminopropyl)-N'-ethylcarbodiimide hydrochloride; FTIR: Fourier transform infrared spectroscopy; GelMA: Gelatin methacryloyl; MAA: Methacrylic anhydride; NHS: N-hydroxysuccinimide; NMR: Nuclear magnetic resonance; PBA: Phenylboronic acid; PBA@G: PBA-modified gelatin; PVA: Polyvinyl alcohol; SEM: Scanning electron microscopy.

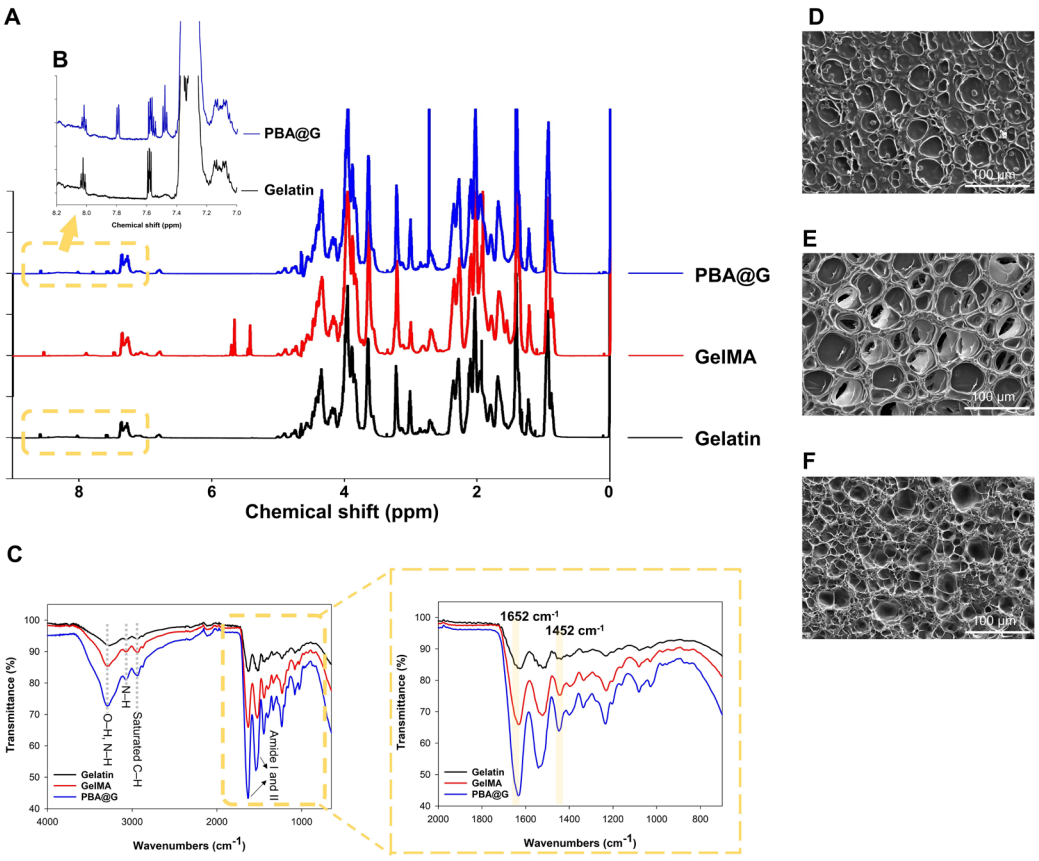


Figure 2. Characterization of GelMA and PBA@G. (A) 1H NMR spectra of gelatin, GelMA, and PBA@G recorded in D_2O at 37 °C. (B) Comparison of the NMR signals between gelatin and PBA@G. (C) FTIR spectra of gelatin, GelMA, and PBA@G measured at room temperature in attenuated total reflection mode. SEM images of (D) GelMA, (E) 10G10P, and (F) 10G10P1PVA hydrogels. Scale bar: 100 μm; magnification: 350×.
Abbreviations: FTIR: Fourier transform infrared spectroscopy; GelMA: Gelatin methacryloyl; NMR: Nuclear magnetic resonance; PBA@G: Phenylboronic acid–modified gelatin; SEM: Scanning electron microscopy.

After freeze-drying, the SEM images of three different mixed formulations were compared (Figure 2D–F). All three materials exhibited porous structures following freeze-drying. Compared with the GelMA formulation, the 10G10P formulation had smaller pores. After the addition of 1% PVA (10G10P1PVA), the pores decreased further in size and became more uniform, producing a denser microstructure than that observed in GelMA. Because SEM was performed after freeze-drying, these images characterize pore morphology but do not directly establish hydrogel mechanical strength. PBA groups can form dynamic boronate ester bonds with the diol groups of PVA. These reversible interactions may contribute to the rheological behavior of the composite hydrogel.

3.2. Rheological properties, transparency, swelling properties, and degradation of the compounds *in vitro*

As shown in Figure 3A–B, the sol–gel transition temperatures (G′ = G″) for gelatin, GelMA, PBA@G, 10G10P, and 10G10P1PVA were 33.44 °C, 32.28 °C, 33.66 °C, 33.00 °C, and 34.23 °C, respectively, indicating that all formulations were in the gel state at room temperature (25 °C). Amplitude sweep testing was used to compare the rheological response of the formulations under the tested shear conditions. The measured shear stress values for gelatin and PBA@G were 1,344 and 1,397 Pa, respectively, whereas that of GelMA was 630.7 Pa; 10G10P and 10G10P1PVA showed values of 5,589 and 4,270 Pa, respectively. These measurements were used for formulation comparison and were not interpreted as direct measures of hydrated tensile, fracture, or implantation-related mechanical strength. The parent material used in this work was type A gelatin with a bloom factor of 300.[38]

Spectral scanning of photocrosslinked 10G10P1PVA at 37 °C showed that transmittance increased from 44.57% to 66.22% across the measured range of 400–700 nm, while letters remained visible through the hydrogel as a qualitative reference (Figure 3C). The swelling ratios of lyophilized 10% GelMA, 10G10P, and 10G10P1PVA were 1,134.54 ± 84.72%, 711.94 ± 16.99%, and 609.61 ± 101.59%, respectively (Table S2). Thus, inclusion of PBA@G and PVA reduced swelling relative to GelMA alone under the tested conditions. Degradation of 10G, 10G10P, and 10G10P1PVA was evaluated in 1× PBS containing 20 μg/mL type IV collagenase at 37 °C (Figures 3D and S3).

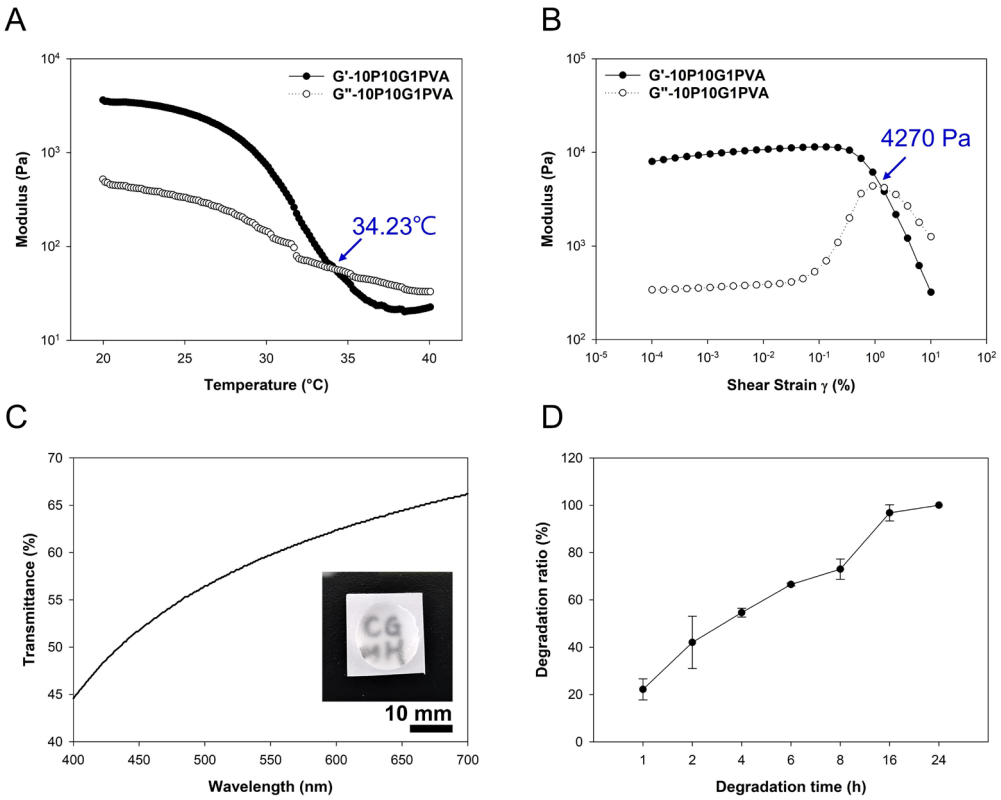


Figure 3. Rheological analysis of 10G10P1PVA using (A) temperature-ramp and (B) amplitude-sweep experiments at 20 °C. (C) Optical transmittance spectrum of photocrosslinked 10G10P1PVA at 37 °C over 400–700 nm. Scale bar: 10 mm; magnification: 1×. (D) Accelerated *in vitro* degradation of 10G10P1PVA in 1× phosphate-buffered saline containing 20 μg/mL type IV collagenase at 37 °C.

Approximately 50% degradation occurred after 6 h, and complete degradation was observed by 24 h. Because this assay was performed under an accelerated enzymatic condition, these data reflect susceptibility to collagenase-mediated degradation rather than the *in vivo* residence time of the hydrogel. The persistence of the implanted construct was not directly quantified in the present study.

The present rheological measurements support formulation comparison for extrusion printing, while hydrated tensile, fracture, fatigue, and suture-related properties remain relevant to implantation-related mechanical assessment. The programmed single-layer height was 0.205 mm, similar in order of magnitude to the approximately 150 μm of anterior stroma removed in the rabbit ALK model. However, the construct was not designed as an exact thickness-matched reconstruction, and actual hydrated construct thickness was not quantitatively measured. Quantitative line width, hydrated thickness, dimensional deviation, and construct–defect geometric matching remain relevant to further evaluation of print fidelity and implantation geometry.

3.3. Viability and phenotypic characteristics of corneal stromal cells in GelMA-based hydrogels

Corneal stromal cells were encapsulated in three GelMA-based hydrogel formulations, 10G, 10G10P, and 10G10P1PVA, and cultured for seven days (Figure 4A). Live/Dead staining performed immediately after photopolymerization (day 0) showed comparable cell survival among the three formulations (10G, 59.00%; 10G10P, 66.52%; and 10G10P1PVA, 72.00%). Cell viability ranged from 56.17% to 66.79% on day 1 and from 64.82% to 78.15% on day 7 across the three formulations. Although viability increased numerically in the 10G group by day 7, live/dead staining alone does not distinguish cell proliferation from changes in the proportion of surviving cells; therefore, metabolic activity was evaluated independently using CCK-8.

The day-7 CCK-8 assay provided a quantitative assessment of cellular metabolic activity. Relative to the 10G group, which was normalized to 100%, the 10G10P and 10G10P1PVA groups showed relative CCK-8 levels of 144.98 ± 23.69% and 137.23 ± 11.92%, respectively (Figure 4A). The 10G10P group was numerically higher than 10G but did not reach statistical significance ($p = 0.058$), whereas the 10G10P1PVA group exhibited significantly greater metabolic activity than 10G ($p = 0.020$). Together with the live/dead staining results, these data indicate that incorporation of PBA@G and PVA did not compromise CSC viability during the 7-day culture period and that the 10G10P1PVA formulation supported higher day-7 metabolic activity than GelMA alone.

Because the elongated morphology observed in the composite hydrogels could not distinguish cell spreading from fibroblastic or myofibroblastic activation, cytoskeletal organization and phenotype-associated gene expression were further examined on day 7 (Figure 4B). Phalloidin staining showed limited spreading of CSCs in 10G, whereas cells in 10G10P and 10G10P1PVA displayed a more elongated morphology with F-actin bundles predominantly oriented along the longitudinal axis of the cells; this organization was most evident in 10G10P1PVA. Quantitative RT-PCR provided molecular context for these morphological observations. *ACTA2* (α-SMA) expression was significantly increased in the myofibroblast-like reference population (CSC-M), whereas all three hydrogel groups remained at low *ACTA2* expression without the pronounced induction observed in CSC-M. In contrast, *ALDH3A1*, encoding a keratocyte-associated corneal crystallin, was reduced in CSC-M and in the B4G12 negative control. Among the hydrogel groups, *ALDH3A1* expression was similar between 10G and 10G10P but was significantly higher in 10G10P1PVA. Taken together, 10G10P1PVA supported CSC survival, metabolic activity, cell spreading, and a phenotype-associated marker profile during the seven-day culture period.

Cellular responses to the matrix must be considered in cell-laden corneal constructs. CSC morphology is strongly influenced by the culture environment and does not reliably distinguish keratocyte, fibroblastic, and myofibroblastic states. We therefore evaluated cell viability, metabolic activity, F-actin organization, and phenotype-associated gene expression rather than relying on morphology alone.[25,26]

Live/Dead staining and the CCK-8 assay provided complementary, nonconflicting information. Comparable live/dead viability assays indicated that the proportion of viable cells was similar among formulations, whereas the higher CCK-8 signal in 10G10P1PVA indicated greater overall metabolic activity. Because the CCK-8 signal reflects both viable cell number and cellular metabolic state, this finding cannot be interpreted alone as increased cell proliferation. Phalloidin staining confirmed cell spreading and longitudinal F-actin organization within the construct. These features indicate cell–matrix interaction and cytoskeletal adaptation but do not define CSC phenotype. *ALDH3A1* expression was higher in CSCs cultured in 10G10P1PVA than in those cultured in 10G or 10G10P. ALDH3A1 is a corneal crystallin expressed by native keratocytes and is reduced when human keratocytes acquire fibroblastic or myofibroblastic repair phenotypes.[39] Because the same CSC source and culture conditions were used across formulations, this difference suggests that 10G10P1PVA provided an environment that better

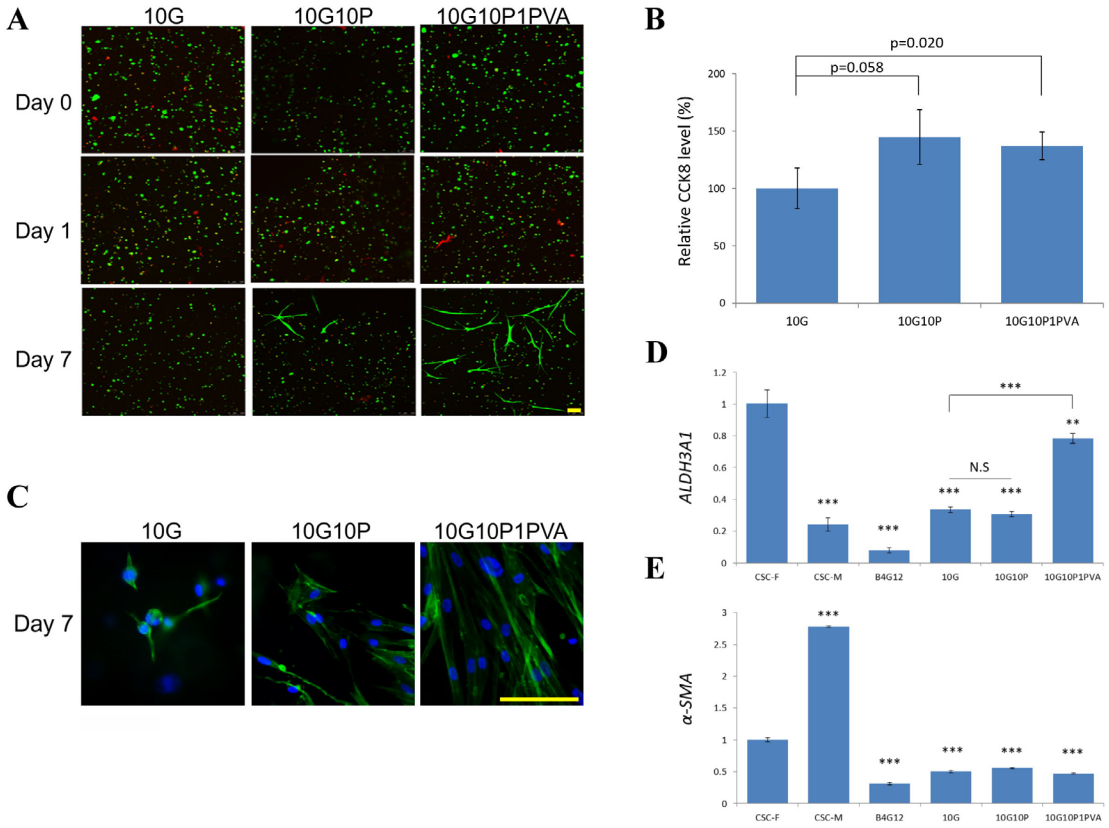


Figure 4. Viability, cytoskeletal organization, and phenotypic marker expression of human corneal stromal cells (CSCs) cultured in GelMA-based hydrogels. (A) Representative live/dead staining images of CSCs cultured in 10G, 10G10P, and 10G10P1PVA hydrogels on days 0, 1, and 7. Live cells are shown in green and dead cells in red. Cell viability remained within a similar range among the three hydrogel formulations at the assessed time points. Scale bar: 100 μm; magnification: 100×. (B) Cellular metabolic activity was quantified using CCK-8 on day 7 and normalized to the 10G group. The 10G10P group was higher than 10G but did not reach statistical significance (p = 0.058), whereas 10G10P1PVA showed significantly higher metabolic activity than 10G (p = 0.020). (C) Representative day-7 phalloidin staining of F-actin (green) with DAPI nuclear counterstaining (blue). CSCs in 10G10P and 10G10P1PVA exhibited greater spreading and longitudinal F-actin organization than those in 10G. Scale bar: 100 μm; magnification: 200×. Quantitative RT-PCR analysis of (D) *ALDH3A1* and (E) *ACTA2* (encoding α-SMA) expression. CSC-F and CSC-M groups are included as phenotypic reference populations; separate characterization of these reference states is shown in Figure S4. B4G12 was included as a negative control for *ALDH3A1*. *ALDH3A1* expression was significantly higher in 10G10P1PVA than in 10G and 10G10P, whereas the hydrogel groups did not exhibit the marked *ACTA2* induction observed in CSC-M. Quantitative RT-PCR data are presented as mean ± SD.
Notes: $^{**}p < 0.01$ and $^{***}p < 0.001$; N.S: Not significant.
Abbreviations: α-SMA: Alpha-smooth muscle actin; CCK-8: Cell Counting Kit-8; DAPI: 4′,6-diamidino-2-phenylindole; GelMA: Gelatin methacryloyl; PBA@G: Phenylboronic acid–modified gelatin; RT-PCR: Real-time polymerase chain reaction.

supported *ALDH3A1* expression. The comparison with 10G10P suggests that inclusion of PVA, or the resulting PBA–PVA network, may have contributed to this response, although the responsible matrix property cannot be identified from the present data.

The higher *ALDH3A1* expression in 10G10P1PVA was considered together with CSC survival, metabolic activity, cell spreading, and the observed low *ACTA2* expression relative to CSC-M. This combined pattern indicates a more favorable short-term CSC response to 10G10P1PVA among the tested hydrogels. However, a higher expression of a single marker does not establish stable maintenance of the keratocyte phenotype. The present data therefore describe phenotype-associated responses observed during the seven-day culture period rather than stable phenotype control.

Given the potential relationship between stromal cell state and matrix remodeling, CSCs cultured under conditions intended to limit myofibroblastic activation (CSC-F) or induce a myofibroblast-like state (CSC-M) were characterized separately (Figure S4). CSC-F and CSC-M showed distinct morphologies and α-SMA band intensities, while MMP-2 levels were higher in CSC-M. These observations indicate that the culture

conditions generated distinguishable reference states. Corneal keratocytes, fibroblasts, and myofibroblasts have distinct transcriptional programs and matrix-remodeling characteristics.[40] MMP activity has also been shown to participate in corneal keratocyte spreading, migration, and local extracellular matrix remodeling in 3D collagen matrices[41] The present reference experiment did not test how either state affected the hydrogel. These *in vitro* reference states were not extrapolated to molecular expression in rabbit corneal tissue after implantation.

3.4. Corneal healing after anterior lamellar keratectomy in rabbits

The 10G10P1PVA hydrogel was evaluated in a rabbit ALK model over a seven-day postoperative period. Following removal of the corneal epithelium and anterior stroma, the defects were left without grafting (Control) or treated with an allogeneic corneal graft (Graft), a cell-free 10G10P1PVA hydrogel (Cell-Free), or a 10G10P1PVA hydrogel containing RCSCs (Cell-Full). External eye photographs and fluorescein staining were used to monitor postoperative recovery (Figure 5). Mild central corneal haze remained visible during the seven-day observation period, whereas no additional gross ocular abnormalities were apparent on external examination. On day 4, fluorescein retention remained evident in the Control, Cell-Free, and Cell-Full groups, whereas little to no retention was observed in the Graft group. By day 7, fluorescein retention was no longer apparent in the Control, Graft, and Cell-Full groups, whereas residual staining remained detectable in the Cell-

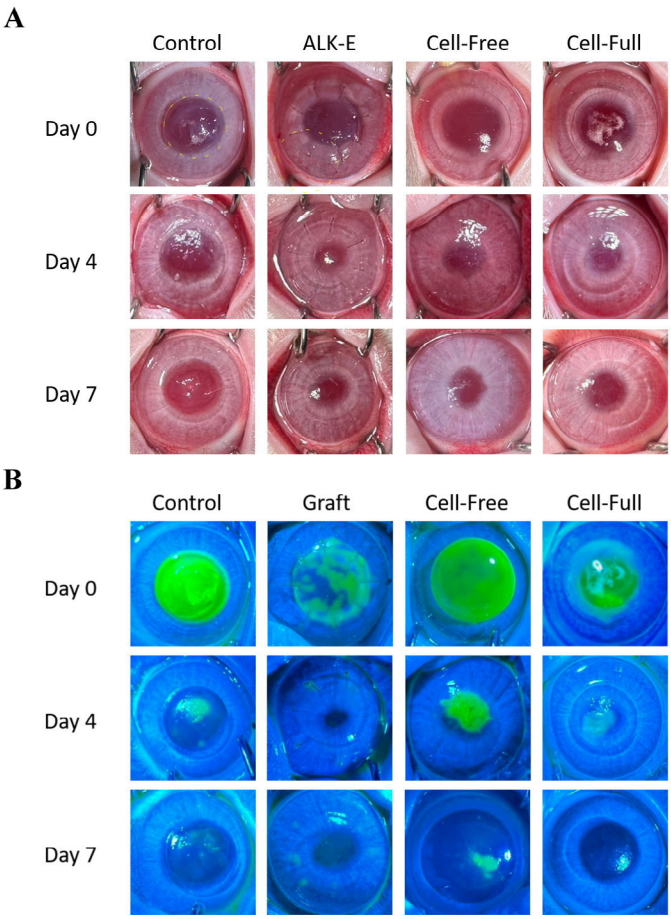


Figure 5. Corneal healing after anterior lamellar keratectomy (ALK) in rabbits. (A) External eye photographs and (B) fluorescein sodium staining images are shown for the Control, Graft, Cell-free, and Cell-Full groups. Images were obtained on days 0, 4, and 7 after ALK, as indicated from top to bottom within each panel. Day 0 images were obtained after the respective treatment was placed and before temporary amniotic membrane coverage. Yellow dashed circles in the day 0 external photographs indicate the ALK area. The Control group underwent ALK without grafting, whereas the Graft, Cell-Free, and Cell-Full groups received an allogeneic corneal graft, a cell-free 10G10P1PVA hydrogel, and a rabbit CSC-seeded 10G10P1PVA hydrogel, respectively. On day 4, fluorescein retention remained evident in the Control, Cell-Free, and Cell-Full groups, whereas little to no retention was observed in the Graft group. By day 7, fluorescein retention was no longer apparent in the Control, Graft, and Cell-Full groups, whereas residual staining remained detectable in the Cell-Free group.

Free group. Because fluorescein staining primarily reflects epithelial barrier integrity, these observations support short-term differences in epithelial barrier recovery rather than overall corneal healing.

All ALK groups received temporary amniotic membrane coverage and eyelid closure to protect the surgical area and implanted constructs during the early postoperative period. Amniotic membrane has been reported to provide a substrate for epithelial migration and re-epithelialization and to contain bioactive components that modulate inflammation and wound healing.[42] We therefore cannot exclude a shared effect of the amniotic membrane on the early healing environment during the first three days. However, the membrane and eyelid sutures were removed on day 3 in all ALK groups, making this a common early postoperative condition. Under this shared condition, the lower fluorescein retention observed in the Cell-Full group than in the Cell-Free group at day 7 supports the possibility that CSCs may have provided an additional contribution to early corneal repair.

The difference between the Cell-Full and Cell-Free groups may reflect biological activity of the incorporated RCSCs in addition to the hydrogel scaffold. Corneal repair involves coordinated epithelial–stromal interactions, and stromal cells can influence epithelial migration and proliferation through paracrine signaling and extracellular matrix remodeling.[26,43] Hepatocyte growth factor and keratinocyte growth factor are well-characterized mediators of stromal-to-epithelial signaling in the cornea.[43] The RCSC-containing construct may therefore provide temporary cell delivery and a local cellular microenvironment during the early postoperative period. The accelerated *in vitro* degradation assay does not define the *in vivo* persistence of the construct, and a day-7 difference does not require the hydrogel to remain intact throughout the entire seven-day period. Within the present observation window, the lower fluorescein retention in the Cell-Full group than in the Cell-Free group supports a potential contribution of the cellular component to early repair. Longer-term follow-up with standardized slit-lamp haze grading, optical coherence tomography–based corneal thickness measurements, and corneal topography will be important to evaluate later stromal remodeling and the stability of corneal transparency, thickness, and curvature.

3.5. Histological analysis

Masson's trichrome staining was performed to evaluate corneal tissue organization seven days after ALK (Figure 6). These sections were used for morphological comparison of tissue architecture rather than quantitative pachymetric measurement; therefore, absolute postoperative corneal thickness was not inferred from the histological sections. Morphologically, the Normal group showed a full-thickness corneal profile, whereas the Control group showed a thinner tissue profile with an irregular anterior corneal contour after removal of the epithelium and approximately 150 μm of the anterior stroma. The Graft group exhibited a relatively smooth anterior surface and a visible graft–host interface. No complete hydrogel layer could be clearly identified in the day-7 sections of the Cell-Free and Cell-Full groups. In the Cell-Free group, the anterior contour remained markedly irregular with an uneven stromal profile, whereas the Cell-Full group showed a smoother anterior contour and more uniform stromal architecture. Continuous epithelial coverage was present in all ALK groups at day 7, although epithelial thickness and organization did not uniformly resemble those of the normal cornea. No conspicuous dense inflammatory cell

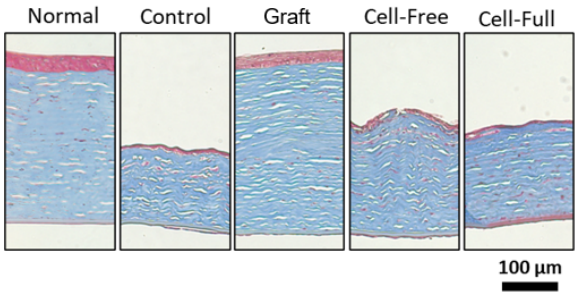


Figure 6. Histological evaluation of corneal healing after anterior lamellar keratectomy (ALK). Representative Masson's trichrome-stained corneal sections are shown for the Normal, Control, Graft, Cell-Free, and Cell-Full groups. Corneas from the four ALK groups were harvested seven days after surgery, with normal cornea included as a reference. The Control group underwent ALK without grafting, whereas the Graft, Cell-Free, and Cell-Full groups received an allogeneic corneal graft, a cell-free 10G10P1PVA hydrogel, and an RCSC-seeded 10G10P1PVA hydrogel, respectively. The sections were used for morphological comparison rather than quantitative pachymetric measurement. Continuous epithelial coverage was present in all ALK groups. The Cell-Free group exhibited a markedly irregular anterior contour and uneven stromal profile, whereas the Cell-Full group showed a smoother anterior contour and more uniform stromal architecture. No conspicuous dense inflammatory cell accumulation was apparent in the representative hydrogel-treated sections. Scale bar: 100 μm; magnification: 100×.

accumulation was apparent within the stromal tissue in the representative sections.

The more regular tissue architecture in the Cell-Full group compared with the Cell-Free group, together with the lower fluorescein retention observed on day 7, supports a potential additional contribution of the RCSC-containing construct during early corneal repair. Because all ALK groups received the same temporary amniotic membrane coverage and eyelid closure, these differences occurred under a common postoperative healing condition. Masson's trichrome staining does not identify specific inflammatory cell populations or quantify α-SMA or MMP expression, and tissue expression of these markers was not measured in the rabbit corneas in the present study. Accordingly, the histological findings are interpreted in terms of epithelial continuity, anterior corneal contour, and stromal organization rather than tissue-level molecular regulation.

To clarify the position and contribution of the present study within the literature on corneal stromal bioinks and related material systems, representative studies are summarized in Tables 1 and 2. As shown in Table 1, corneal stromal bioinks have been developed using GelMA, corneal decellularized extracellular matrix/GelMA, GelMA/collagen, GelMA/carboxymethyl chitosan, and other composite systems. Table 2 summarizes material and bioprinting precedents directly relevant to the GelMA/PBA@G/PVA design, including PVA-containing corneal hydrogels, PBA-functionalized gelatin/PVA boronate ester hydrogels, boronate ester–based printable bioink, and PBA-modified GelMA systems. These studies establish prior use of PVA in corneal hydrogels, PBA–diol dynamic networks, boronate-mediated crosslinking in printable GelMA-containing bioink, and PBA-modified GelMA. For extrusion-based corneal stromal bioprinting, however, a bioink must exhibit rheological behavior compatible with extrusion and, after printing, maintain construct geometry in an aqueous environment while providing a cell-compatible microenvironment. PBA@G and PVA can form a reversible boronate ester network through PBA–diol interactions. We therefore incorporated this dynamic network into GelMA to modulate rheological and hydration behavior while retaining GelMA photocrosslinking. Among the studies summarized, related material chemistries and boronate-based printable systems have been reported in other applications, but the GelMA/PBA@G/PVA combination has not been reported as a CSC-laden corneal stromal bioink. In addition, although some corneal bioink studies have evaluated stromal cell phenotype, the present study incorporated assessment of

Table 1. Representative corneal stromal bioinks: material and biological comparison

Study	Bioink/Fabrication	Material/Printing evaluation	Biological/*In vivo* evaluation
Kim *et al*., 2019[15]	Corneal dECM; shear-guided 3D cell printing	Transparency; collagen fibril alignment	Cell organization; matrix remodeling
Kilic Bektas and Hasirci, 2019[9]	GelMA; keratocyte-laden printing; photocrosslinking	Optical transmission; mechanical properties	Keratocyte viability; stromal phenotype markers
Zhang *et al*., 2023[11]	Corneal dECM/GelMA; digital light processing	Curvature; optical and mechanical properties	Cell viability; epithelial regeneration; matrix alignment
Xu *et al*., 2025[12]	GelMA/collagen; flat and convex 3D-printed constructs	Flat/convex construct architecture	Keratocyte phenotype; fibrosis-related gene/protein expression
Basoz *et al*., 2025[14]	GelMA; cell-loaded and cell-free 3D-printed constructs	Printability; water content; compression; transparency	Rabbit implantation; tissue response
Vijayaraghavan *et al*., 2026[13]	GelMA/carboxymethyl chitosan; cell-laden printing; photocrosslinking	Printability; thermal stability; optical transmission	Keratocyte markers (keratan sulfate, lumican); α-SMA
Present study	GelMA/PBA@G/PVA (10G10P1PVA); CSC-laden extrusion; photocrosslinking	Rheological behavior; swelling; optical transmittance; collagenase degradation; extrusion printability	CSC viability; metabolic activity; *ALDH3A1* and *ACTA2* expression; exploratory *in vivo* evaluation

Abbreviations: α-SMA: Alpha-smooth muscle actin.; CSC: Corneal stromal cell; dECM: Decellularized extracellular matrix; GelMA: Gelatin methacryloyl; PBA: Phenylboronic acid; PBA@G: PBA-functionalized gelatin; PVA: Poly(vinyl alcohol).

Table 2. Material precedents relevant to the GelMA/PBA@G/PVA formulation

Study	Material system	Application	Established precedent
Han *et al*., 2020[44]	Bacterial cellulose/PVA composite	Corneal stromal substitute	CSC compatibility and tissue response
Wang *et al*., 2021[45]	3-CPBA-grafted gelatin/PVA; boronate ester hydrogel	Diabetic wound treatment	Reversible dynamic crosslinking; no cell-laden construct
Feng *et al*., 2022[46]	HAMA-PBA/GelMA/HA-DA; dynamic crosslinking	Tissue adhesion	Boronate-mediated dynamic crosslinking in a GelMA-containing printable bioink
Chou *et al*., 2024[27]	4-CPBA-modified GelMA; photocrosslinking	Vitreoretinal surgery	Biocompatibility; no cell-laden construct
Li *et al*., 2026[47]	PBA-modified alginate/PVA	Corneal drug delivery	Responsive hydrogel behavior; no cell-laden construct

Abbreviations: CPBA: Carboxyphenylboronic acid; CSC: Corneal stromal cell; GelMA: Gelatin methacryloyl; HA-DA: Dopamine-modified hyaluronic acid; HAMA-PBA: Hyaluronic acid modified with methacrylate and phenylboronic acid groups; PBA: Phenylboronic acid; PBA@G: PBA-functionalized gelatin; PVA: Poly(vinyl alcohol).

both keratocyte-associated and myofibroblast-associated phenotypic responses.

The experimental findings support this design strategy. Relative to 10G, 10G10P1PVA showed a different rheological response and lower swelling under the tested conditions, while remaining suitable for extrusion and photocrosslinking into corneal constructs. The change in material composition did not compromise short-term CSC viability. Compared with 10G, 10G10P1PVA showed higher metabolic activity, and *ALDH3A1* expression was higher than in both 10G and 10G10P. Thus, incorporation of PBA@G/PVA altered the material behavior of GelMA and reduced swelling without compromising short-term CSC viability, while being accompanied by higher metabolic activity and *ALDH3A1* expression. The study further extended evaluation of the cell-laden formulation to an exploratory rabbit ALK model, providing short-term *in vivo* observations of epithelial recovery and stromal organization following implantation.

4. Conclusion

In summary, we developed a 10G10P1PVA composite hydrogel and characterized its rheological behavior, optical transmittance, swelling, degradation, printability, and cytocompatibility. Among the tested formulations, 10G10P1PVA supported CSC viability over seven days, greater day-7 metabolic activity than 10G, and higher *ALDH3A1* expression than 10G or 10G10P without the marked *ACTA2* induction observed in CSC-M. The exploratory rabbit ALK evaluation provided short-term qualitative observations of epithelial recovery and stromal organization following implantation. These material and biological results support further evaluation of 10G10P1PVA as a GelMA-based composite bioink for corneal stromal bioprinting.

Acknowledgments

The authors thank the Microscope Core Laboratory, Genomic Medicine Core Laboratory, and Laboratory Animal Center, Chang Gung Memorial Hospital, Linkou branch, for providing technical assistance.

Funding

This study was partially supported by Chang Gung Memorial Hospital (CMRPG3Q0481) for Chen H.C. and the Taiwan National Science and Technology Council Grants (NSTC 114-2314-B-182-002 and 114-2811-B-182-014) for Tsai TT. The funding organization played no role in the design or conduct of this research.

Conflict of interest

Chung-An Chen is an employee of AngenMed Therapeutics, Inc., but was not involved in any activities that could constitute a conflict of interest in relation to this study. The other authors declare that there is no conflict of interest.

Author contributions

Conceptualization: Yi-Jen Hsueh, Chung-An Chen, Tsung-Ting Tsai, Hung-Chi Chen

Formal analysis: Yi-Jen Hsueh, Chung-An Chen

Funding acquisition: Tsung-Ting Tsai, Hung-Chi Chen
Investigation: All authors
Methodology: Yi-Jen Hsueh, Chung-An Chen, Chin-Yu Yang, Chang-Hong Lin, Chun-Yuan Cheng, Chih-Hsin Lin, Shih-Jung Liu
Project administration: Tsung-Ting Tsai, Hung-Chi Chen
Supervision: Tsung-Ting Tsai, Hung-Chi Chen
Validation: Yi-Jen Hsueh, Chung-An Chen, Tsung-Ting Tsai, Hung-Chi Chen
Visualization: Yi-Jen Hsueh, Chung-An Chen
Writing–original draft: Yi-Jen Hsueh, Chung-An Chen
Writing–review & editing: Tsung-Ting Tsai, Hung-Chi Chen

Ethics approval and consent to participate

This research was conducted in accordance with the principles of the Declaration of Helsinki, and it received approval from Chang Gung Memorial Hospital's Institutional Review Board (IRB No. 202001800B0).

Consent for publication

Not applicable.

Availability of data

The datasets generated during and/or analyzed during the current study are available from the corresponding author on reasonable request.

References

1. Gain P, Jullienne R, He Z, *et al*. Global survey of corneal transplantation and eye banking. *JAMA Ophthalmol*. 2016;134(2):167-173.

   doi: 10.1001/jamaophthalmol.2015.4776

2. Guerin LP, Le-Bel G, Desjardins P, *et al*. The human tissue-engineered cornea (hTEC): Recent progress. *Int J Mol Sci*. 2021;22(3):1291.

   doi: 10.3390/ijms22031291

3. Germain L, Auger FA, Grandbois E, *et al*. Reconstructed human cornea produced in vitro by tissue engineering. *Pathobiology*. 1999;67(3):140-147.

   doi: 10.1159/000028064

4. Kim HK. Development of a bioengineered cornea using a 3-dimensional bioprinting system. *Cornea*. 2014;33(S11):S12.

   doi: 10.1097/ico.0000000000000230

5. Li P, Zhang M, Chen Z, Tian B, Kang X. Tissue-engineered injectable gelatin-methacryloyl hydrogel-based adjunctive therapy for intervertebral disc degeneration. *ACS Omega*. 2023;8(15):13509-13518.

   doi: 10.1021/acsomega.3c00211

6. Yue K, Trujillo-de Santiago G, Alvarez MM, Tamayol A, Annabi N, Khademhosseini A. Synthesis, properties, and biomedical applications of gelatin methacryloyl (GelMA) hydrogels. *Biomaterials*. 2015;73:254-271.

   doi: 10.1016/j.biomaterials.2015.08.045

7. Isaacson A, Swioklo S, Connon CJ. 3D bioprinting of a corneal stroma equivalent. *Exp Eye Res*. 2018;173:188-193.

   doi: 10.1016/j.exer.2018.05.010

8. Duarte Campos DF, Rohde M, Ross M, *et al*. Corneal bioprinting utilizing collagen-based bioinks and primary human keratocytes. *J Biomed Mater Res A*. 2019;107(9):1945-1953.

   doi: 10.1002/jbm.a.36702

9. Kilic Bektas C, Hasirci V. Cell loaded 3D bioprinted GelMA hydrogels for corneal stroma engineering. *Biomater Sci*. 2019;8(1):438-449.

   doi: 10.1039/c9bm01236b

10. Kong B, Chen Y, Liu R, *et al*. Fiber reinforced GelMA hydrogel to induce the regeneration of corneal stroma. *Nat Commun*. 2020;11(1):1435.

    doi: 10.1038/s41467-020-14887-9

11. Zhang M, Yang F, Han D, *et al*. 3D bioprinting of corneal decellularized extracellular matrix: GelMA composite hydrogel for corneal stroma engineering. *Int J Bioprint*. 2023;9(5):774.

    doi: 10.18063/ijb.774

12. Xu Y, Liu W, Zhao Q, *et al*. 3D bioprinted GelMA/collagen hydrogel for corneal stroma regeneration. *Biofabrication*. 2025;17(4):045002.

    doi: 10.1088/1758-5090/ade7b2

13. Vijayaraghavan R, Loganathan S, Valapa RB. Functional 3D bioprinting with GelMA/CMCh bioinks: a supportive microenvironment for stromal keratocyte maintenance and potential corneal stromal repair. *J Mater Chem B*. 2026;14(15):4704-4723.

    doi: 10.1039/d5tb02459e

14. Basoz D, Akalinli A, Buyuksungur S, *et al*. Preclinical testing of 3D printed, cell loaded hydrogel based corneal substitutes on rabbit model. *Macromol Biosci*. 2025;25(7):e2400595.

    doi: 10.1002/mabi.202400595

15. Kim H, Jang J, Park J, *et al*. Shear-induced alignment of collagen fibrils using 3D cell printing for corneal stroma tissue engineering. *Biofabrication*. 2019;11(3):035017.

    doi: 10.1088/1758-5090/ab1a8b

16. Gao Y, Peng K, Mitragotri S. Covalently Crosslinked hydrogels via step-growth reactions: crosslinking chemistries, polymers, and clinical impact. *Adv Mater*.

2021;33(25):e2006362.

doi: 10.1002/adma.202006362

17. Nasra S, Patel M, Shukla H, Bhatt M, Kumar A. Functional hydrogel-based wound dressings: A review on biocompatibility and therapeutic efficacy. *Life Sci*. 2023;334:122232.

doi: 10.1016/j.lfs.2023.122232

18. El Sayed MM. Production of polymer hydrogel composites and their applications. *J Polym Environ*. 2023;31(7):2855-2879.

doi: 10.1007/s10924-023-02796-z

19. Lim JYC, Goh L, Otake KI, Goh SS, Loh XJ, Kitagawa S. Biomedically-relevant metal organic framework-hydrogel composites. *Biomater Sci*. 2023;11(8):2661-2677.

doi: 10.1039/d2bm01906j

20. Condo I, Giannitelli SM, Lo Presti D, Cortese B, Ursini O. Overview of dynamic bond based hydrogels for reversible adhesion processes. *Gels*. 2024;10(7):442.

doi: 10.3390/gels10070442

21. Han Y, Cao Y, Lei H. Dynamic Covalent Hydrogels: Strong yet Dynamic. *Gels*. 2022;8(9):577.

doi: 10.3390/gels8090577

22. Perera MM, Ayres N. Dynamic covalent bonds in self-healing, shape memory, and controllable stiffness hydrogels. *Polymer Chemistry*. 2020;11(8):1410-1423.

doi: 10.1039/c9py01694e

23. Chakma P, Konkolewicz D. Dynamic Covalent Bonds in Polymeric Materials. *Angew Chem Int Ed Engl*. 2019;58(29):9682-9695.

doi: 10.1002/anie.201813525

24. Cho S, Hwang SY, Oh DX, Park J. Recent progress in self-healing polymers and hydrogels based on reversible dynamic B–O bonds: boronic/boronate esters, borax, and benzoxaborole. *J Mater Chem A*. 2021;9(26):14630-14655.

doi: 10.1039/d1ta02308j

25. Binte MYNZ, Riau AK, Yam GHF, Binte Halim NSH, Mehta JS. Isolation and propagation of human corneal stromal keratocytes for tissue engineering and cell therapy. *Cells*. 2022;11(1):178.

doi: 10.3390/cells11010178

26. Kamil S, Mohan RR. Corneal stromal wound healing: Major regulators and therapeutic targets. *Ocul Surf*. 2021;19:290-306.

doi: 10.1016/j.jtos.2020.10.006

27. Chou HD, Chen CA, Liu HY, *et al*. Synthesis, properties, and biocompatibility of 4-carboxyphenyboronic acid-modified gelatin-methacryloyl: a hydrogel for retinal surgeries. *ACS Omega*.2024;9(41):42147-42158.

doi: 10.1021/acsomega.4c02842

28. Shirahama H, Lee BH, Tan LP, Cho NJ. Precise tuning of facile one-pot gelatin methacryloyl (GelMA) synthesis. *Sci Rep*. 2016;6(1):31036.

doi: 10.1038/srep31036

29. Liu C, Yu Q, Yuan Z, *et al*. Engineering the viscoelasticity of gelatin methacryloyl (GelMA) hydrogels via small "dynamic bridges" to regulate BMSC behaviors for osteochondral regeneration. *Bioact Mater*. 2023;25:445-459.

doi: 10.1016/j.bioactmat.2022.07.031

30. Habeeb AF. Determination of free amino groups in proteins by trinitrobenzenesulfonic acid. *Anal Biochem*. 1966;14(3):328-336.

doi: 10.1016/0003-2697(66)90275-2

31. Hsueh YJ, Meir YJ, Lai JY, *et al*. Lysophosphatidic acid improves corneal endothelial density in tissue culture by stimulating stromal secretion of interleukin-1beta. *J Cell Mol Med*. 2020;24(12):6596-6608.

doi: 10.1111/jcmm.15307

32. Walejewska E, Melchels FPW, Paradiso A, *et al*. Tuning physical properties of GelMA hydrogels through microarchitecture for engineering osteoid tissue. *Biomacromolecules*. 2024;25(1):188-199.

doi: 10.1021/acs.biomac.3c00909

33. Clerkin S, Singh K, Davis JL, *et al*. Tuneable gelatin methacryloyl (GelMA) hydrogels for the directed specification of renal cell types for hiPSC-derived kidney organoid maturation. *Biomaterials*. 2025;322:123349.

doi: 10.1016/j.biomaterials.2025.123349

34. Xie W, Zhang Y, Zhang J, *et al*. Dynamically crosslinked protien hydrogel composite as multifunctional wound dressing for cutaneous infection. *Colloids Interface Sci Commun*. 2022;50:100654.

doi: 10.1016/j.colcom.2022.100654

35. Li X, Chen S, Li J, *et al*. 3D culture of chondrocytes in gelatin hydrogels with different stiffness. *Polymers*. 2016;8(8):269.

doi: 10.3390/polym8080269

36. Ghosh RN, Thomas J, B. R V, *et al*. An insight into synthesis, properties and applications of gelatin methacryloyl hydrogel for 3D bioprinting. *Mater Adv*. 2023;4(22):5496-5529.

doi: 10.1039/d3ma00715d

37. Krishnamoorthy S, Noorani B, Xu C. Effects of encapsulated cells on the physical-mechanical properties and microstructure of gelatin methacrylate hydrogels. *Int J Mol Sci*. 2019;20(20):5061.

doi: 10.3390/ijms20205061

38. Pepelanova I, Kruppa K, Scheper T, Lavrentieva A. Gelatin-methacryloyl (GelMA) hydrogels with defined degree of functionalization as a versatile toolkit for 3D cell culture and extrusion bioprinting. *Bioengineering*. 2018;5(3):55.

doi: 10.3390/bioengineering5030055

39. Pei Y, Reins RY, McDermott AM. Aldehyde dehydrogenase (ALDH) 3A1 expression by the human keratocyte and its repair phenotypes. *Exp Eye Res*. 2006;83(5):1063-1073.

doi: 10.1016/j.exer.2006.05.011

40. Poole K, Iyer KS, Schmidtke DW, Petroll WM, Varner VD. Corneal keratocytes, fibroblasts, and myofibroblasts exhibit distinct transcriptional profiles in vitro. *Invest Ophthalmol Vis Sci*. 2025;66(3):28.

doi: 10.1167/iovs.66.3.28

41. Zhou C, Petroll WM. MMP regulation of corneal keratocyte motility and mechanics in 3-D collagen matrices. *Exp Eye Res*. 2014;121:147-160.

doi: 10.1016/j.exer.2014.02.002

42. Sanders FWB, Huang J, Alio Del Barrio JL, Hamada S, McAlinden C. Amniotic membrane transplantation: structural and biological properties, tissue preparation, application and clinical indications. *Eye*. 2024;38(4):668-679.

doi: 10.1038/s41433-023-02777-5

43. Wilson SE, Liu JJ, Mohan RR. Stromal-epithelial interactions in the cornea. *Prog Retin Eye Res*. 1999;18(3):293-309.

doi: 10.1016/s1350-9462(98)00017-2

44. Han Y, Li C, Cai Q, *et al*. Studies on bacterial cellulose/poly(vinyl alcohol) hydrogel composites as tissue-engineered corneal stroma. *Biomed Mater*. 2020;15(3):035022.

doi: 10.1088/1748-605X/ab56ca

45. Wang Y, Wu Y, Long L, *et al*. Inflammation-responsive drug-loaded hydrogels with sequential hemostasis, antibacterial, and anti-inflammatory behavior for chronically infected diabetic wound treatment. *ACS Appl Mater Interfaces*. 2021;13(28):33584-33599.

doi: 10.1021/acsami.1c09889

46. Feng Q, Li D, Li Q, *et al*. Assembling microgels via dynamic cross-linking reaction improves printability, microporosity, tissue-adhesion, and self-healing of microgel bioink for extrusion bioprinting. *ACS Appl Mater Interfaces*. 2022;14(13):15653-15666.

doi: 10.1021/acsami.2c01295

47. Li S, Hu X, Zhang G, *et al*. ROS-triggered disassembly of nanoparticle-networked hydrogels enables dynamic gating of corneal tight junctions. *ACS Appl Mater Interfaces*. 2026;18(31):42273-42288.

doi: 10.1021/acsami.6c06859